Journal of Petroleum Science and Engineering 167 (2018) 329–342

Contents lists available at ScienceDirect

Journal of Petroleum Science and Engineering

journal homepage: www.elsevier.com/locate/petrol

Prediction of asphaltene precipitation risk in oil wells using coupled thermohydraulics model

Eissa Al-Safran

Petroleum Engineering Department, Kuwait University, Kuwait

ARTICLE INFO

Keywords:
Asphaltene precipitation
Two-phase flow
Asphaltene instability
Parametric study

ABSTRACT

Asphaltene precipitation and deposition is a major flow assurance challenge, which manifests itself in reservoir, production tubing, and flowline and process facility. Asphaltene may precipitate due to two main factors, namely high asphaltene content, and high difference between reservoir pressure and oil bubble-point pressure, i.e. precipitation driving force, even if asphaltene content is low. The objective of this study is to develop a predictive simulation tool to assess the risk of asphaltene precipitation in oil wells and to estimate the asphaltene risk window. Further objective is to use the developed simulation tool to generate well design and production scenarios to efficiently prevent, mitigate and manage asphaltene precipitation. A comprehensive asphaltene deposition workflow is developed to identify the major steps to enable a solution strategy. To implement the workflow, Ansari et al. (1994) mechanistic two-phase flow hydrodynamic model in vertical wells is coupled with two Asphaltene precipitation thermodynamic models, namely de Boer et al. (1995), and Wang et al. (2006). In this study, de-Boer et al. model is extended from a single point reservoir model to a multi-point wellbore model; while Wang et al. is used to predict and compare the asphaltene instability with live-oil instability along wellbore. The developed simulator was validated to predict the risk and depth window of asphaltene precipitation in Middle East oil wells, resulting in a reasonable agreement with the field data. In addition, the simulation tool is used to carry out a parametric study to investigate the impact of oil gravity, and reservoir pressure on asphaltene precipitation risk.

1. Introduction and literature review

Asphaltene deposition is a serious problem in the oil industry, which manifests itself over the entire production system including reservoir, production, transportation and processing system components. With petroleum industry trend toward exploration and production of deep reservoirs, and heavy asphaltic resources, the challenge of asphaltene deposition increases, which may threatens projects economics and safety. In wellbores, asphaltene deposition may result in production loss by partial or complete plugging of production tubing. To avoid complete production tubing plugging, a continuous monitoring and cleaning is required. Furthermore, plugging of sub-service safety valve (SSSV) and their actuation mechanism, x-tree valves, and other downhole equipment, such as electrical submersible pump may result in serious safety concerns. Asphaltene deposition in surface facilities is also serious flow assurance issue, which might be catastrophic. Asphaltene may deposit not only inside separators and treaters, but also on safety, process, and monitoring systems including indication equipment, high-pressure safety devices, and relief valves. Therefore, an early prediction of asphaltene deposition at surface facilities will save human and financial project assets.

Three major hydrocarbon fractions exists in crude oil systems, namely asphaltene, resins, and wax. While the physical and chemical properties of wax are somewhat understood, the properties of resins and asphaltene are still ambiguous (Firoozabadi, 1999). The amount of asphaltene in crude oil depends on several factors such as the source of the crude, burial depth, API gravity of the crude, and the sulfur content (Speight, 1991). An asphaltic system is considered colloidal system with no volatile fractions. Such asphaltic system consists of three components, namely, asphaltene (dispersed phase), resins (peptizing agent), and oil (the dispersion medium) (Yen, 1995). Although there is no universally agreed upon definition of asphaltene, the classic definition of asphaltene is based on its solubility in a specific solvent. Therefore, asphaltene is defined as insoluble in normal alkanes such as *n*-pentane, and soluble in excess benzene and toluene (Firoozabadi, 1999), and is a dark brown to black friable solid that has no definite melting point and decomposes leaving a carbonaceous residue under heating (Mansoori, 1997). Although not much is known about the chemistry of asphaltene, the knowledge of asphaltene chemistry is essential in providing accurate chemical properties and thereby accurate characterization and modeling. Asphaltene consists of hydrocarbon molecules such as

E-mail address: e.alsafran@ku.edu.kw.

https://doi.org/10.1016/j.petrol.2018.04.024
Received 1 January 2018; Received in revised form 8 April 2018; Accepted 12 April 2018
Available online 14 April 2018
0920-4105/

hydrogen and carbon, and hetero elements, i.e. oxygen, nitrogen and sulfur. Differences in the asphaltene composition from one region to another are anticipated due to the different maturation processes and the nature of the source. A comparison of elemental composition of asphaltene from worldwide sources indicates that the hydrogen to carbon ratio (H/C) varies over 0.05–1.15 %wt. On the other hand, data shows a notable variation in the content of hetero-elements, namely oxygen content which ranges from 0.3 to 4.9 %wt., and sulfur content which ranges from 0.3 to 10.3 % wt. Nitrogen content is relatively less, and varies from 0.6 to 3.3 % wt. The elemental composition data clearly shows that the change in composition of asphaltene is due to variation of hetero-elements content and not hydrocarbons molecules (Speight, 1991). Determination of actual molecular structure of asphaltene was found difficult due to the complexity of its molecules. Nevertheless, asphaltene consists of aromatic nuclei that contains alkyl and alicyclic (naphthenic) systems, and hetero elements (nitrogen, oxygen, and sulfur) are scattered in different locations. Determination of accurate molecular weight of asphaltene is also a challenge. The low solubility of asphaltene in solvents used in molecular weight measurement, and the presence of adsorbed resin in asphaltene are the two main challenges to determine asphaltene molecular weight. The reported molecular weight of asphaltene varies within 1000–2,000,000, which depends on the method of determination as well as measurement conditions. Therefore, a careful precipitation of the asphaltene to extract all resin and the right choice of the measurement method are key factors for reliable molecular weight determination (Speight, 1991).

In asphaltene deposition, the asphaltic system thermodynamic state is crucial to study the behavior of asphaltene precipitation under any given temperature, pressure and compositional conditions. Asphaltene phase behavior envelope is a p-T plot that shows the thermodynamics conditions under which asphaltene solid particles precipitate. On the other hand, the locus of points at which the asphaltene flocculate (aggregate) is called Asphaltene Deposition Envelop (ADE). The determination of the boundaries of ADE is a challenging task. For example, ADE does not have a critical point because a critical point requires a bubble point and a dew point lines; however, ADE does not have dew point line because asphaltene does not vaporize at high temperature, yet it disintegrates. Therefore, ADE consists of bubble point line only, and upper and lower ADE boundaries (Leontaritis, 1989). Asphaltene flocculation process is known to be irreversible, which means that once the upper ADE boundary is crossed and asphaltene flocculates, reversing the thermodynamic path will not de-flocculate the asphaltene (Leontaritis, 1989). On the other hand, Hirschberg et al. (1984) questioned the fact that asphaltene irreversibility depends on how titration experiments is conducted. For example, when additional precipitant is added after asphaltene precipitate, asphaltene precipitation process will not be reversed because the re-dissolution requires more equilibration time. In addition, in a previous experimental work, Hirschberg et al. (1984) observed that after asphaltene precipitate, it starts dissolving as the pressure increases from 280 to 1000 bar. An explanation for this contradictory behavior is that asphaltene perception is thermodynamically reversible, while flocculation could be either reversible or irreversible, depending on the nature of the crude. In oil field operations, asphaltene flocculation process is seen irreversible due to the large size of asphaltene flocs and their adsorption affinity to solid surfaces, sand, and fine particles, which may not wash away by chemical remediation techniques (Mansoori, 1997).

Four major factors control the onset and amount of asphaltene deposition, namely pressure, temperature, oil composition and flow condition/conduit material, i.e. Electrokinetics effect. The temperature affects the internal energy and the density of the liquid phase, which subsequently affects oil-phase solubility parameter (Burke et al., 1990). Therefore, as the temperature increases, oil phase density decreases, and solubility to resins increases, resulting in resin transfer from micelles (a polar structure of asphaltene particle surrounded by resin particles) to oil phase. Consequently, the attractive force of micelles increases due to the exposure of polar asphaltene particles, leading to asphaltene flocculation. However, the effect of temperature is found to be insignificant (Takhar et al., 1995). System pressure has a minimal effect on asphaltene precipitation above bubble point pressure where oil composition is constant, while it has significant effect at and below bubble point pressure (MacMillan et al., 1995). Above bubble point, decreasing system pressure has the same effect of increasing temperature described above. On the other hand, below bubble point, pressure decrease increases the oil density, which disturbs resins equilibrium, resulting in resins migrating from micelles to oil phase. This will expose polar asphaltene particles, leading to asphaltene flocculation and deposition (Burke et al., 1990). Asphaltene precipitation also depends on oil composition, i.e. introducing n-alkanes into the system upsets resin concentration equilibrium, transferring the resin from micelles to the oil phase, which promotes asphaltene flocculation and deposition (Takhar et al., 1995). Finally, as asphaltic crude oil flows in metallic conduit, an electrical potential difference may be generated due to charged particles motion and friction. Consequently, generated electrokinetic field increases the colloidal particles polarity, leading to asphaltene particle attraction and flocculation. The generated electrokinetics potential depends the flow regime, i.e. laminar vs. turbulent, asphaltene polarity and structure, and conduit thermal and electrical characteristics (Mansoori, 1997).

Several investigators developed prediction simulation tools by modeling the asphaltene thermodynamics behavior under static lab condition. However, hydrodynamic flow condition has a significant effect on both asphaltene precipitation, and more importantly on asphaltene particles transportation, entrainment, and deposition. Kabir and Jamaluddin (2002) developed a pragmatic, cost-effective, and environmental friendly solution to mitigate tubular asphaltene deposition in south Kuwait wells. A thermodynamic fluid characterization of the crude oil was carried out based on which they proposed a mitigation solution, which consists of a 20% of a de-asphalted oil with 1% dispersant (in volume), which ensured asphaltene solubility along the entire production string according to their field tests. Alkafeef et al. (2005) developed a simple method to predict the asphaltene deposition onset under flow condition, as well as the deposit thickness. A verification study of their method against data acquired in west Kuwait field shows a reasonable agreement. Abdallah et al. (2010) investigated asphaltene deposition in onshore wells located in Abu Dhabi by intensive thermodynamic fluid characterization, which is used to calibrate a thermodynamic based simulator to study the effect of process and production conditions on asphaltene stability. In their study, an EOS is used to model the asphaltene phase behavior, and kinetic and transport models to model the deposition behavior. Kurup et al. (2012) developed a simulation tool to predict the location and amount of asphaltene deposits in wellbores. Alapati and Joshi (2013) developed an efficient field method to test chemical inhibitors and dispersants, which does not require high-pressure reservoir samples, thus it is cost effective, and time efficient. Sulaimon and Govindasamy (2015) developed an empirical correlation to predict asphaltene deposition tendency in Malaysian crude oil. Their correlation is based on the Colloidal Instability Index, Refractive Index and molecular weight of both oil and lumped fraction of crude oil. Abuie et al. (2015) modeled asphaltene deposition in wells operating under gas lift, using a comprehensive thermal compositional wellbore model. The prediction shows that injecting light gas composition promotes asphaltene precipitation in the well. Hashmi and Firoozabadi (2016) conducted a lab-scale capillary experiment to study the removal mechanism of asphaltene deposits. In their study, three chemical inhibitors were used to reverse/remove asphaltene deposits. Among the three, the strong organic surfactant dodecyl-benzene-sulfonic acid is found to be the most effective to remove asphaltene deposits and with concentration of ten times less than that required by toluene.

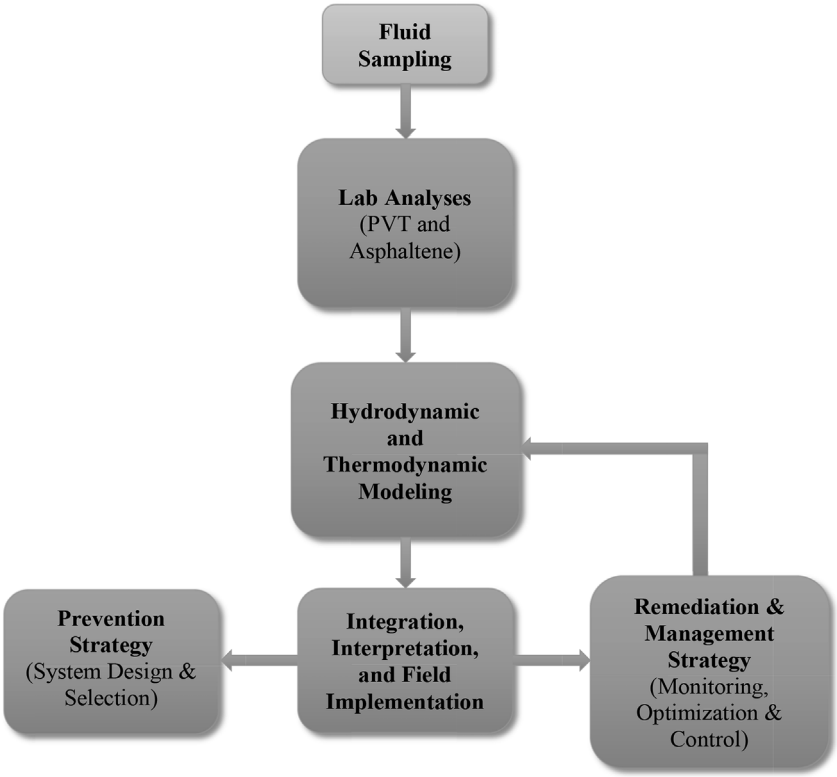

Fig. 1. Integrated asphaltene workflow process.

2. Asphaltene deposition integrated workflow

In this study, an integrated workflow process is developed to analyze the problem of asphaltene deposition and come up with a strategy for a solution. Fig. 1 shows the integrated asphaltene deposition workflow, which enables a strategy of prevention, remediation and management of asphaltene deposition. This process is essential in early stage of field development to ensure proper management or flow assurance risks.

Sampling reservoir fluids is important first step of asphaltene deposition proper management on which all subsequent steps depend. Representative samples of oil, and gas from multiple depths and aerial locations of reservoir are required to understand the compositional variation of the fluids. This is followed by lab analyses including pressure, volume, and temperature (PVT) analysis and characterization of asphaltene. The objective of PVT analysis is to determine the conditions of phases change, volume, composition, and properties of each phase. Understanding fluid behavior is a key factor in asphaltene deposition risk assessment, and management. Although PVT analysis is conducted over a limited range of pressures and temperatures, it is used to validate, select and tune mass transfer PVT models to predict the fluid behavior along the production systems and for different times. Asphaltene characterization includes a dead oil SARA (Saturate, Aromatic, Resin, Asphaltene) analysis, paraffinic solvent titration for asphaltene stability screening, and one live-oil asphaltene onset pressure. If potential risks arise, an Asphaltene Precipitation Envelope (APE) is generated. In this study the onset solubility parameter of the asphaltene and its temperature are required as an input data for Wang et al. (2006) thermodynamic model.

The hydrodynamic and thermodynamic modeling step of Fig. 1 provides a holistic view of the production system behavior and its interaction with asphaltene deposition. The objective of modeling the hydrodynamic behavior of a production system is to determine the pressure, temperature, flow pattern, liquid holdup, and flow rate profiles. Hydrodynamic modeling is carried out using a black-oil and compositional mass transfer models, and steady-state mechanistic modeling to provide pressure and fluids phase/properties profiles along the wellbore. In this study, we used a simple linear temperature gradient model that should be provided by the user. The predicted pressure, temperature, and fluid properties along the well are then used in the thermodynamic model to predict the risk of asphaltene precipitation. The integration, interpretation and field implementation step of asphaltene deposition workflow integrates and interprets the previous steps to assess asphaltene precipitation risk and production system operability. Accordingly, system design or remediation/management strategies (or both) to prevent or manage, respectively, the impact of asphaltene precipitation risk are selected.

In the prevention strategy option, system design strategies, including system layout, flowline and choke sizing, choke location, separation facility sizing, thermal management, chemical injections requirements, and pigging operations are considered and implemented. A well-engineered system design based on fluids characterization and flow behavior simulations pays off during the operation stage where it will become easy to manage asphaltene deposition risks. The remediation and management strategy involves monitoring the production system to provide feedback on possible asphaltene deposition risk and the required operational procedures to remediate and manage them through system optimization. Such feedback and control can be a direct input to hydrodynamic and thermodynamic modeling to improve the operability of the system and minimize asphaltene risk.

3. Modeling

The modeling part of this study consists of three main models, namely mass transfer, hydrodynamic, and thermodynamic models. In this study, two mass transfer models have been used to characterize the fluid and predict its composition, and properties, namely Kartoatmodjo and Schmidt (1991) black-oil model and Peng-Robinson (1976) Equation of State (EOS) compositional model. The predicted parameters are used to calculate the in-situ flow rates, two-phase flow pattern, liquid

holdup, and pressure gradient using the two-phase flow hydrodynamic. These parameters are then used in the thermodynamic models to predict asphaltene precipitation. In this study, Ansari et al. (1994) mechanistic model is used to predict flow behavior and hydrodynamics including flow pattern, liquid holdup, and pressure gradient along the wellbore. To model the asphaltene precipitation, two thermodynamic models have been used in this study, namely de Boer et al. (1995) and Wang et al. (2006). The details of the mathematical formulation of the three models are presented in Appendix A.

It is important to note that the mass transfer, two-phase flow, and thermodynamic models used in this study are not purely empirical based models, yet they are mechanistic models, which combines conservation laws as well as empirical relationship. Therefore, these models can predict asphaltene precipitation for wide range of input conditions with reasonable accuracy and confidence. It is possible to tune these models whenever experimental data is available for any of the parameters in the three models.

4. Simulation description

A simulator is developed based on the mass transfer, hydrodynamic, and thermodynamic modeling, using a numerical scheme of average pressure method with forward marching algorithm. The wellbore is discretized into segments and sections, where the average pressure and all its defendant variables such as phases fluid properties, phases flow rates, flow pattern etc. are iterated in each segment from the bottom-hole to wellhead. Fig. 2 shows the flow chart of the simulator solution procedure. The simulator requires several input data, including fluid and asphaltene properties, production and reservoir data, and well geometrical data as shown in Table 1.

The simulator outputs consists the pressure, temperature, and liquid holdup profiles along the wellbore. In addition, profiles of fluid properties that are required in the thermodynamics model are also generated, for quality and reliability check. The main output of the simulator are a modified wellbore de-Boer et al. plot, and a modified Wang et al. asphaltene solubility plot. To illustrate the simulator output results, the simulator was executed for an actual well data, where asphaltene deposition have been encountered. Fig. 3 shows the asphaltene precipitation prediction using de-Boer et al. model, which predicts the risk of asphaltene precipitation along the entire well. The simulator prediction of live oil density along the well shows two different profiles, namely oil density below and above bubble point pressure. Furthermore, the simulator predicts three regions of asphaltene precipitation, namely no asphaltene, slight asphaltene, and severe asphaltene. For the given case in Fig. 3, de-Boer et al. model predicts no asphaltene precipitation from 0 to 600 ft, and slight risk of asphaltene precipitation from 600 ft to the bottom of the well.

Fig. 4 shows the prediction of Wang et al. model along the entire well. Two profiles are generated, namely the asphaltene solubility parameter at instability condition, and live-oil solubility parameter profiles. As the live-oil solubility parameter along the well becomes lower than the asphaltene onset solubility, i.e. it intersects the asphaltene solubility parameter, asphaltene precipitation is predicted with the highest risk at bubble point pressure as shown by the peak of the live-oil solubility parameter at around 10,000 ft. Conversely, if the live-oil solubility is larger than that of the asphaltene onset solubility during depressurization from reservoir condition, asphaltene is stable and no precipitation is predicted. This simulation result does not only predict the risk of asphaltene precipitation, but also the highest risk location and depth window. In this case, it is predicted to be from 5300 ft to the bottom of the well i.e. End Of Tubing (EOT), which fairly concedes with the conducted slick-line tubing check test of this well, which indicated the asphaltene deposition occurs from 3650 ft to the End Of Tubing (EOT).

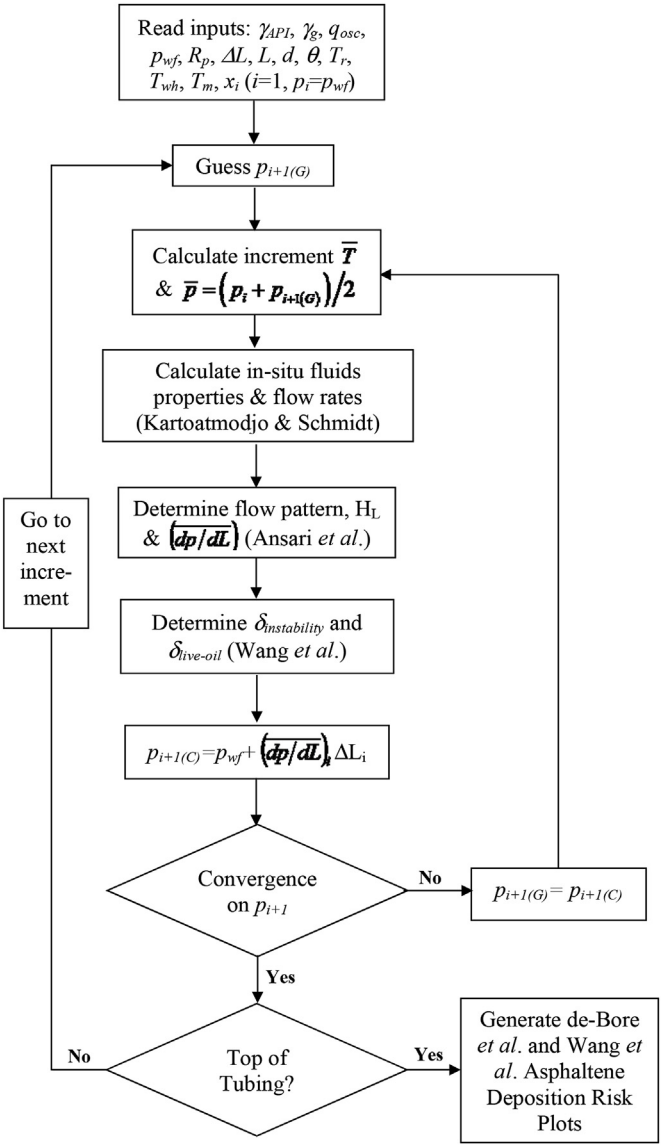

Fig. 2. Flow chart of simulation solution procedure.

Table 1
Simulation input data.

Parameters	Unites
Specific Gravity (gg)	–
API Gravity (gAPI) Deg.	Deg.
Composition (C1-C6)	–
Onset solubility parameter	MPa0.5
Temp at onset solubility parameter	Deg. C
Oil flow rate	STBO
Flowing bottomhole pressure	psi
Produced GOR	scf/STB
Reservoir pressure	psi
Reservoir temperature	Deg. C
Wellhead temperature	Deg. C
Tubing ID	in.
Well inclination angle	Deg.
Well depth	ft.
Tubing roughness	in.

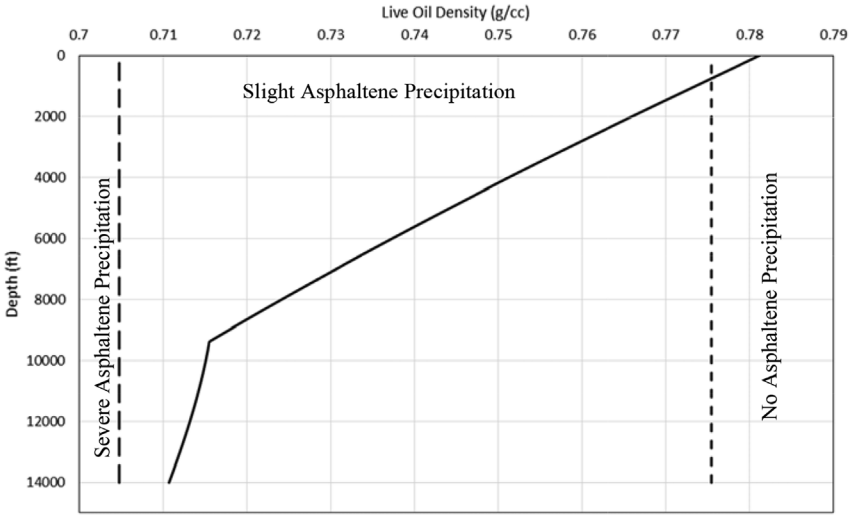

Fig. 3. Simulation prediction using de-Boer et al. model.

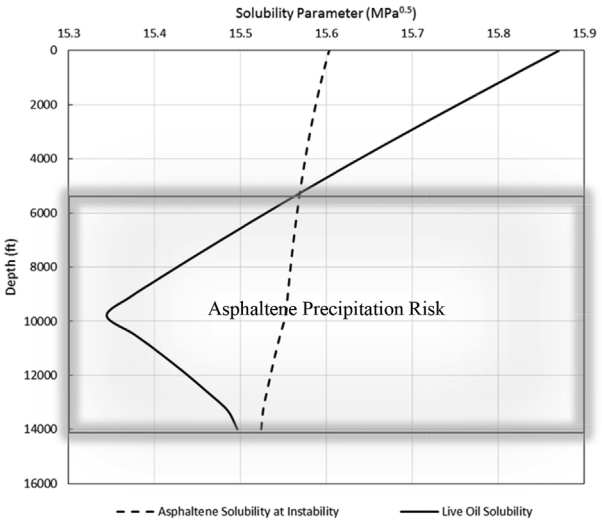

Fig. 4. Simulation prediction using Wang et al. model.

5. Validation study

Four Middle East field cases have been used to validate the model and simulator predictions developed in this study. These cases are from the same reservoir, but from three different fields, indicating slight differences in fluid properties and flow rates. For each case, fluid characterization analyses have been acquired from PVT reports, reservoir and production data from well test data, and well geometry from completion data. The simulator is executed for each field case to determine the risk of asphaltene precipitation using de-Boer et al. and Wang et al. methods.

5.1. Fluid characterization analyses

The fluid property data required for the validation is obtained from PVT reports, where bottom-hole fluid samples were collected and analyzed to obtain the fluid PVT properties, which are required as input to the simulator. The fluid characterization analysis in the PVT reports includes first validity and quality checks of the sample. A constant mass study (P-V relation) was performed at reservoir temperature using pressurized PVT cell to determine relative volume, compressibility, and saturation pressure. In addition, compositional analysis study involved

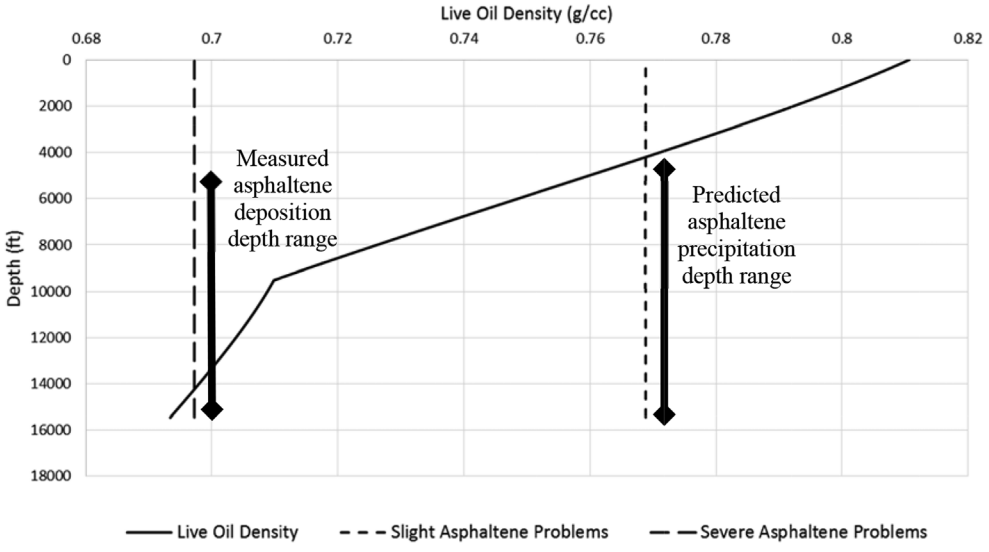

Fig. 5. Simulation validation of de-Boer et al. model (field case well A).

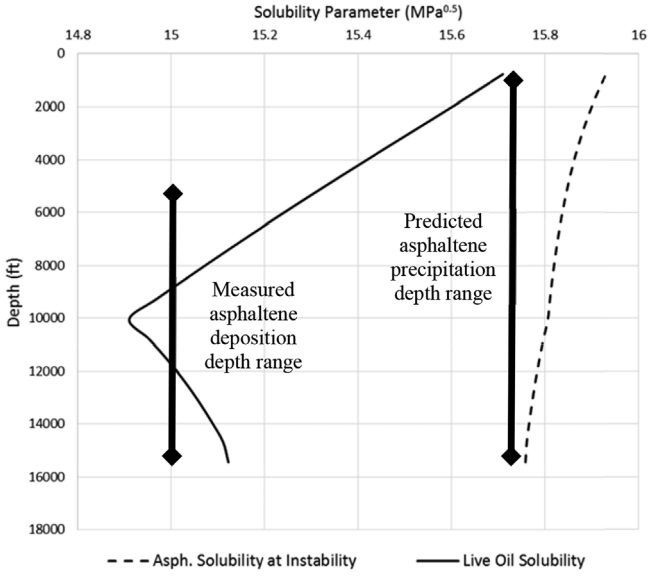

Fig. 6. Simulation validation of Wang et al. model (Field case well A).

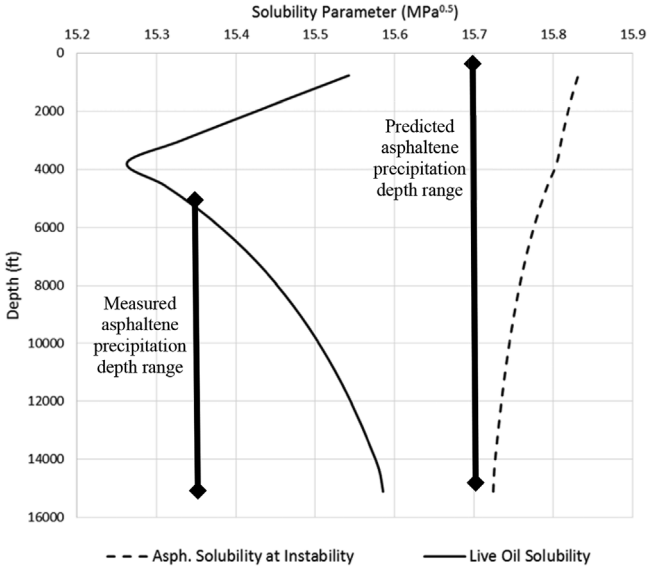

Fig. 8. Simulation validation of Wang et al. model (Field case well B).

a controlled atmospheric flash at reservoir temperature to measure the gas-liquid ration and both flashed gas and flashed liquid compositions, using gas chromatography. A differential liberation test at reservoir temperature is carried out to simulate the fluid behavior during reservoir depletion process, where the pressure is incrementally reduced below bubble point pressure. At each equilibrium pressure step, the oil and gas volumes at both reservoir and standard conditions are measured. Using electromagnetic viscometer, the fluid dynamic viscosity at reservoir temperature, and wide range of pressures below and above bubble point pressures is measured. Finally, part of the fluid sample is subjected to measure the fluids phase fraction and composition at separator condition.

5.2. Field case well A

Fig. 5 shows de-Boer et al. model prediction of asphaltene precipitation risk in well A. The simulator predicted a severe asphaltene risk at the bottom of the well, and a slight risk from 4188 to 14,216 ft. The field data reported that a slick line tool measures asphaltene deposition 4921 to 15,450 ft, indicating a close match with the simulator prediction.

The simulator prediction of asphaltene precipitation risk using Wang et al. model for well A is shown in Fig. 6. In this case, asphaltene precipitation risk is predicted along the entire well as the live-oil solubility parameter profile crosses the entire asphaltene solubility parameter at instability profile. Furthermore, Wang et al. model prediction indicates that the highest asphaltene precipitation risk is located around depth of 10,000 ft, where the asphaltene solubility parameter is the highest close to bubble point pressure, which matches the field measurement. This highest risk location can be used as a guidance of the location of chemical injection to optimize the asphaltene clean out.

5.3. Field case well B

Fig. 7 shows the validation results of well B, using de-Boer et al. model, which predicts asphaltene precipitation risk along the entire well. The simulator prediction also shows that the risk increases at the bottom of the well and close to the bubble-point pressure located approximately at 4000 ft. The asphaltene deposition field data shows that asphaltene deposition is measured by a slick-line tool from 5026 to the end of tubing (EOT), which partially matches the simulator prediction.

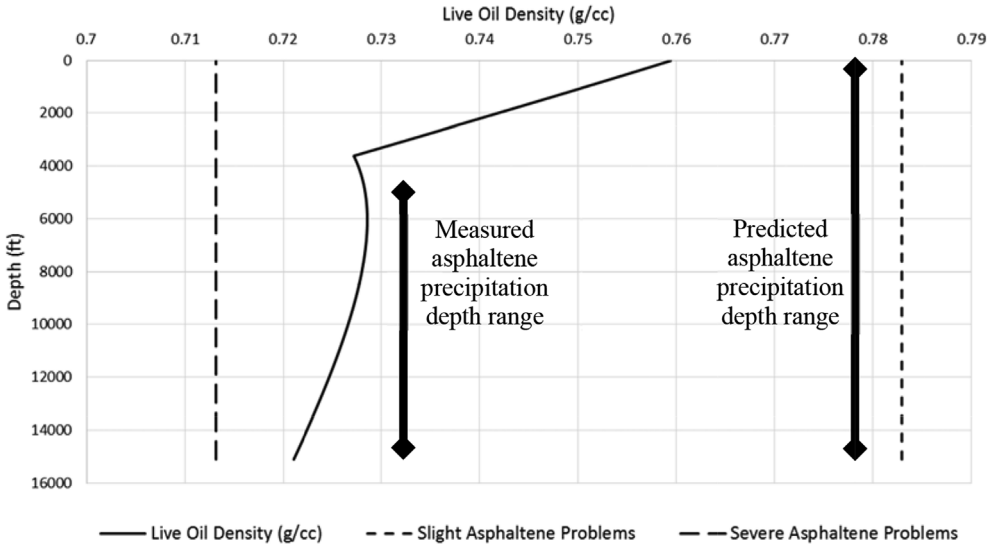

Fig. 7. Simulation validation of de-Boer et al. model (field case well B).

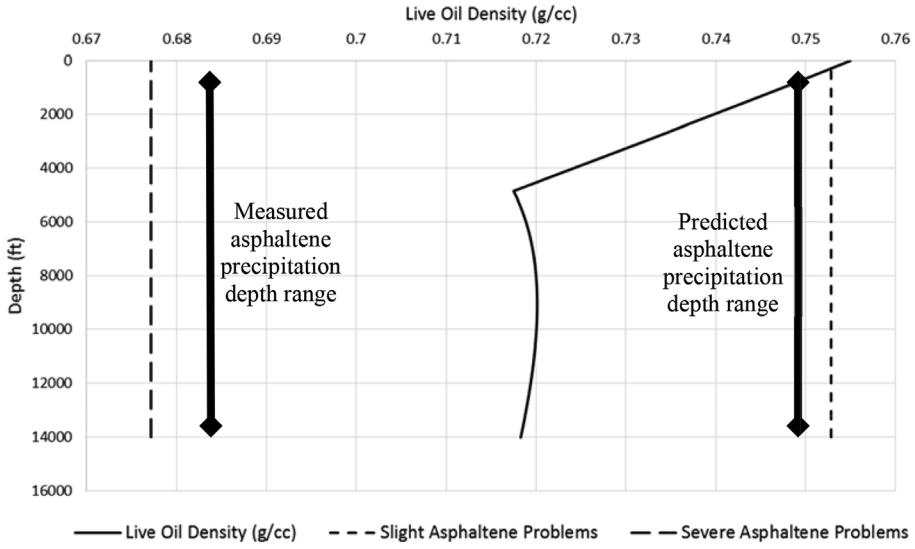

Fig. 9. Simulation validation of de-Boer et al. model (field case well C).

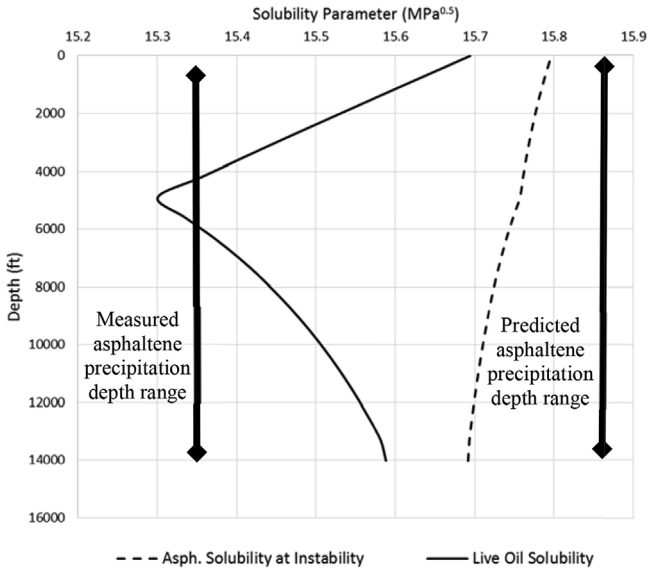

Fig. 10. Simulation validation of Wang et al. model (Field case well C).

Fig. 8 is the simulator prediction of asphaltene precipitation risk, using Wang et al. model, which predicts asphaltene precipitation risk along the entire well. The asphaltene cleanout report indicates that slick-line measured asphaltene deposition from 5026 ft to the EOT. Although the field data partially matches the prediction, model prediction of the highest asphaltene precipitation risk at 4000 ft does not match the field measurement.

5.4. Field case well C

Fig. 9 shows the validation of the simulation prediction using de-Boer et al. model, which predicts slight asphaltene precipitation approximately along the entire well. The field data shows that asphaltene deposition was observed from 90 ft to EOT, using a slick-line tool. This indicates a close match with the simulator prediction. Wang et al. model validation is given in Fig. 10, which predicts asphaltene precipitation along the entire well, matching the field data of asphaltene deposition from 90 ft to EOT. Furthermore, Wang et al. model prediction shows that the highest risk of asphaltene precipitation is at a depth of 5000 ft, which can be used to design the optimum injection point for chemical treatment.

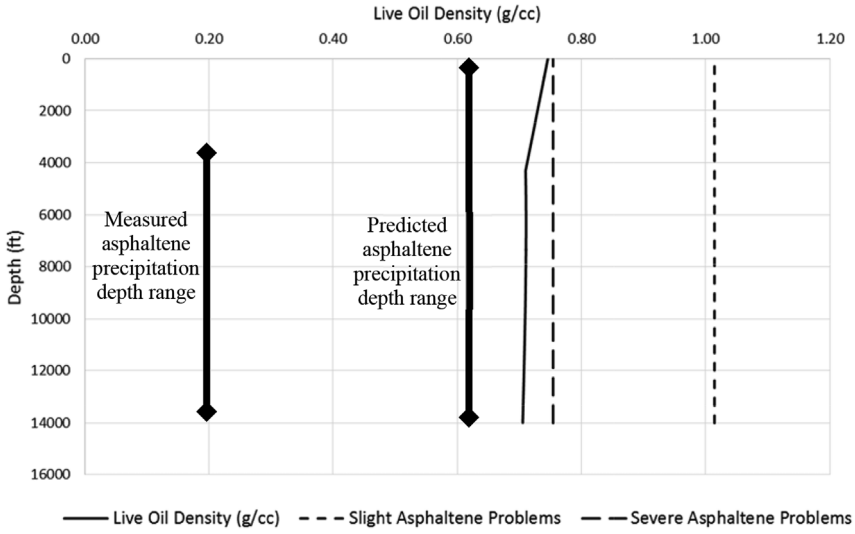

Fig. 11. Simulation validation of de-Boer et al. model (field case well D).

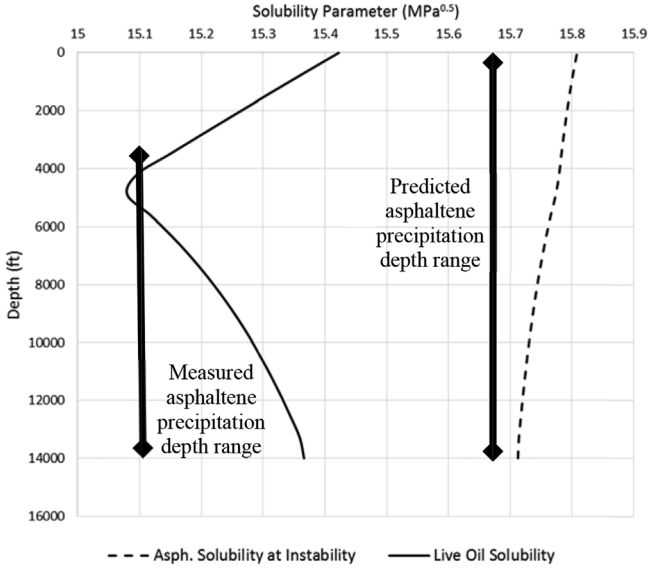

Fig. 12. Simulation validation of Wang et al. model (Field case well D).

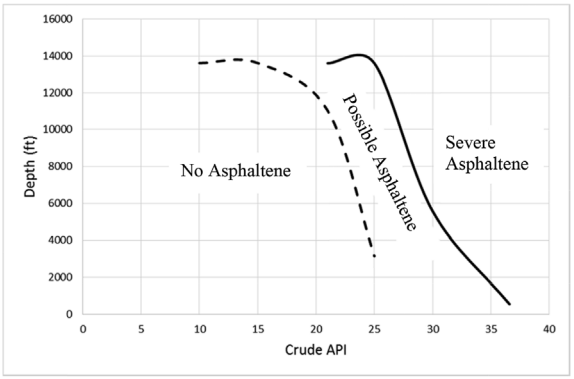

Fig. 13. Effect of oil API gravity on asphaltene precipitation along wellbore.

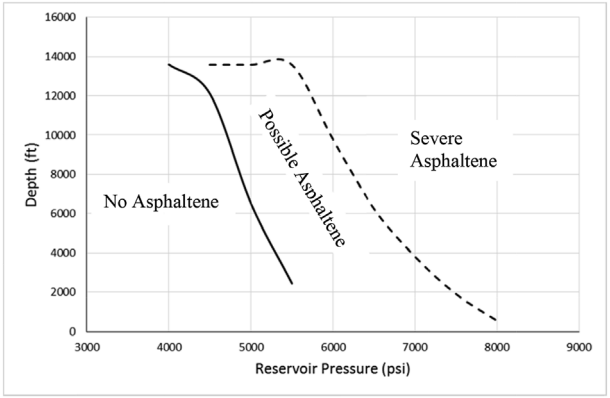

Fig. 14. Effect of reservoir pressure on asphaltene precipitation along wellbore.

5.5. Field case well D

Fig. 11 shows the simulation results of de-Boer et al. model, predicting a severe asphaltene precipitation along the entire well. Similar, the field data using slick-line indicated that asphaltene deposits from 3650 ft to the EOT, partially matching the simulator prediction.

Wang et al. model prediction shown in Fig. 12 shows asphaltene precipitation along the entire tubing. Furthermore, Wang et al. model prediction indicates that the highest asphaltene precipitation risk is located around depth of 5000 ft, which coincide with the field measurement of asphaltene deposition. The cleanout field report indicated that asphaltene deposition from 3650 ft to the EOT. The predicted high-risk location of asphaltene deposition can provide guideline for efficient chemical treatment and optimal design.

6. Simulation parametric study

Using the developed simulator, a preliminary parametric study is carried out to investigate the impact of system parameters on the risk of asphaltene precipitation. Two parameters have been investigated, namely crude oil API gravity, and reservoir pressure. The simulator is executed for several values of each parameter, with all other parameters constants. Fig. 13 shows the effect of API gravity on asphaltene precipitation along the wellbore, where it shows that as API gravity increases, asphaltene precipitation risk increases. This behavior is attributed to the fact that a light crude oil has high bubble point pressure, resulting in an early asphaltene precipitation as pressure drops in wellbore. This information is critical in designing miscible HC/CO_2 EOR method, and gas lift artificial method, which both have effect on the crude oil composition, i.e. API gravity. Fig. 14 shows the simulation result of the effect of reservoir pressure on asphaltene precipitation, which shows that as reservoir pressure increases, asphaltene precipitation tendency increases. This trend is attributed to the fact that as reservoir pressure increase, the pressure driving force (p_{res}-p_b) to precipitate asphaltene increases, as indicated in de Boer et al. (1995) model. This information is important in designing reservoir pressure maintenance technique, such as waterflooding to minimize any risk of possible asphaltene precipitation.

7. Conclusions

Asphaltene precipitation in oil wells is investigated in this study. A comprehensive workflow process to model, prevent, mitigate, or manage asphaltene deposition in wells is developed to identify the major steps of solution strategy. A simulation tool is developed in this study using coupled thermodynamic (Wang et al. and de-Boer et al.) modeling and hydrodynamic two-phase flow (Ansari et al.) model. In addition, fluid characterization and properties along the wellbore are modeled using black-oil model and compositional (EOS) model. The models were coupled and solved numerically, using average pressure method with forward marching algorithm along the wellbore. The developed simulator predictions were validated with four Middle East wells data, which shows good agreement in term of the asphaltene precipitation risk, and the approximate depth window of highest risk location of asphaltene precipitation, which can be used as guidance for field chemical treatment injection operation. To investigate the effect of crude API gravity and reservoir pressure on asphaltene precipitation, a parametric study is carried out using the developed simulator, which shows that as API gravity and reservoir pressure increase, the risk of asphaltene precipitation increases. This knowledge is important in designing miscible HC/CO_2 EOR methods, gas-lift artificial lift application, and designing pressure maintenance technique such as waterflooding.

Appendix A. Models Mathematical Formulation

The modeling part of this study consists of three main models, namely mass transfer, hydrodynamic, and thermodynamic models. The following is detail mathematical formulation of each model.

Mass transfer modeling

In this study, two mass transfer have been used to calculate fluid properties, hydrodynamic and thermodynamic parameters, namely Kartoatmodjo and Schmidt (1991) Black Oil mass transfer model and the Compositional model. The Black Oil model is used to predict fluid phase behavior for fluid of GOR < 2000 scf/STB, while the Compositional model is used for fluids of GOR > 2000. Several important physical fluid properties are predicted by the model along simulated wells, which are used to calculate the in-situ flow rates, pressure gradient, liquid holdup and inputs into the thermodynamic model. Following is a summary of the Kartoatmodjo and Schmidt (1991) model Black Oil and the Compositional models.

Black oil model

The units system used in Kartoatmodjo and Schmidt (1991) model black oil is field units.Solution gas-oil ratio and bubble point pressure. For $\gamma_{API} \leq 30$

$$R_s = 0.05958\,\gamma_{g100}^{0.7972}\,p^{1.0014}\,10^{13.1405\gamma_{API}/(T+460)} \tag{A1}$$

$$p_b = \left(\frac{R_p}{0.05958\,\gamma_{g100}^{0.7972}\,10^{13.1405\gamma_{API}/(T+460)}}\right)^{0.9986} \tag{A2}$$

for $\gamma_{API} > 30$

$$R_s = 0.03150\,\gamma_{g100}^{0.7587}\,p^{1.0937}\,10^{11.289\gamma_{API}/(T+460)} \tag{A3}$$

$$p_b = \left(\frac{R_p}{0.03150\,\gamma_{g100}^{0.7587}\,10^{11.289\gamma_{API}/(T+460)}}\right)^{0.9143} \tag{A4}$$

where,

$$\gamma_{g100} = \gamma_g\left[1.00 + 0.1595\gamma_{API}\,T_{sep}^{-0.2466}\log\frac{p_{sep}}{114.7}\right] \tag{A5}$$

Formation volume factor (FVF). *Below bubble point pressure*

$$B_o = 0.98496 + 0.0001F^{1.5} \tag{A6}$$

where

$$F = R_s^{0.755}\gamma_{g100}^{0.25}\gamma_o^{-1.5} + 0.45T \tag{A7}$$

For FVF above bubble point pressure the following correlation is used,

$$B_o = B_{ob}\exp[c_o(p_b - p)] \tag{A8}$$

where,

$$c_o = \frac{6.8257\times10^{-6}}{p}R_S^{0.5002}\gamma_{API}\,T^{0.7606}\gamma_{g100}^{-0.35505} \tag{A9}$$

Crude oil viscosity. To determine the live oil viscosity, the dead-oil viscosity is required first, which is calculated as follows,

$$\mu_{od} = (16.0\times10^8)T^{-2.8177}(\log\gamma_{API})^{5.7526\log(T)-26.9718} \tag{A10}$$

Live oil viscosity below bubble point pressure

$$\mu_o = -0.06821 + 0.9824f + 0.0004034f^2 \tag{A11}$$

where

$$f = \left(0.2001 + 0.8428\left(10^{-0.000845R_s}\right)\right)\mu_{od}^{(0.43+0.5165y)} \tag{A12}$$

and

$$y = 10^{-0.00081R_s} \tag{A13}$$

Above bubble point pressure

$$\mu_o = 1.00081\mu_{ob} + 0.001127(p - p_b)(-0.006517\mu_{ob}^{1.8148} + 0.038\mu_{ob}^{1.590}) \tag{A14}$$

Crude oil density. The crude oil density is an important parameter in the asphaltene deposition thermodynamic modeling. It is calculated using the following equations,

$$\gamma_{gd} = \left[\frac{(\gamma_{API} + 12.5)}{50}\right] - 3.5715\times10^{-6}(\gamma_{API})(R_s) \tag{A15}$$

$$\gamma_{gf} = \frac{R_p\gamma_{gT} - R_s\gamma_{gd}}{R_p - R_s} \tag{A16}$$

$$\rho_{o,live} = \frac{\rho_{w(sc)}\gamma_o + 0.0136R_s\gamma_{gd}}{B_o} \tag{A17}$$

$$\rho_{ob} = \frac{62.4\gamma_o + 0.0136R_p\gamma_{gT}}{B_{ob}} \tag{A18}$$

$$\rho_o = \rho_{ob}\exp[\bar{c}_o(p - p_b)] \tag{A19}$$

Surface tension. Surface tension is required as an input in the hydrodynamic mechanistic model, which is determined as follows,

$$\sigma_o = \sigma_{od}C \tag{A20}$$

where,

$$\sigma_{od_{68^oF}} = 39 - (0.2571)\gamma_{API} \tag{A21}$$

$$\sigma_{od_{100^oF}} = 37.5 - (0.2571)\gamma_{API} \tag{A22}$$

$$\sigma_{od} = \sigma_{68} - \frac{(T - 68)(\sigma_{68} - \sigma_{100})}{32} \tag{A23}$$

$$C = 1.0 - (0.024)p^{0.45} \tag{A24}$$

In-situ oil flow rate. The in-situ oil flow rate at a given pressure and temperature is calculated as follows,

$$q_o = q_{o_{sc}}B_o \tag{A25}$$

Natural gas fluid properties. For gas phase, ideal gas law Equation of State (EOS) has been used to relate pressure, temperature and volume. Based on empirical studies, the equation of state is modified for real gases to include the gas deviation factor or compressibility factor, often called Z-factor, defined as follows.

$$pV_{real} = ZnRT \tag{A26}$$

Several empirical correlations are available to represent the Z-factor. In this study, the Dranchuk and Abu-Kassem (1975) correlation is presented here, which can be expressed as follows.

$$Z = \left(A_1 + \frac{A_2}{T_{pr}} + \frac{A_3}{T_{pr}^3} + \frac{A_4}{T_{pr}^4} + \frac{A_5}{T_{pr}^5}\right)\rho_r + \left(A_6 + \frac{A_7}{T_{pr}} + \frac{A_8}{T_{pr}^2}\right)\rho_r^2 - A_9\left[\frac{A_7}{T_{pr}} + \frac{A_8}{T_{pr}^2}\right]\rho_r^5 + A_{10}(1 + A_{11}\rho_r^2)\left(\frac{\rho_r^2}{T_{pr}^3}\right)\exp(-A_{11}\rho_r^2) + 1.0 \tag{A27}$$

where ρ_r = reduced gas density defined by the following relationship:

$$\rho_r = \frac{0.27\left(p_{pr}\right)}{ZT_{pr}} \tag{A28}$$

The eleven constants $A_1 - A_{11}$ were determined from non-linear regression on 1500 data points from the Standing and Katz (1942) Z-factor chart. These constant coefficients are as follows:

$A_1 = 0.3265$ $A_2 = -1.0700$ $A_3 = -0.5339$ $A_4 = 0.01569$
$A_5 = -0.05165$ $A_6 = 0.5475$ $A_7 = -0.7361$ $A_8 = 0.1844$
$A_9 = 0.1056$ $A_{10} = 0.6134$ $A_{11} = 0.7210$

Gas formation volume factor (FVF). The in-situ volume of one standard cubic foot of gas is the gas formation volume factor. Gas FVF is always much smaller than one, and mathematically, defined as follows.

$$B_g = \frac{V_{g,sc}}{V_{g,insitu}} \tag{A29}$$

Using the real gas law, the gas FVF is reduced to the following form.

$$B_g = 0.0283\left(\frac{ZT}{p}\right) \tag{A30}$$

where B_g = gas formation volume factor, ft^3/scf; p = pressure, psia; and T = absolute temperature, ^oR.

Gas density. Gas density is defined as the mass per unit volume of gas, which can be determined easily from combining the real gas law with the definition of specific gravity of gas as follows.

$$\rho_g = \frac{(2.7)\gamma_g p}{ZT} \tag{A31}$$

where, γ_g = specific gravity of free gas (air = 1); p = pressure of gas, psia; T = absolute temperature of gas, $^\circ R$; Z = real gas deviation factor; R = 10.73, psia ft^3/lbm-mole ^oR.

Gas viscosity. Gas viscosity can be defined as the ability of gas to flow. Lee et al. (1966) method is used for calculation of gas viscosity as follows.

$$\mu_g = 10^{-4} K \exp\left[X\left(\frac{\rho_g}{62.4}\right)^Y\right] \tag{A32}$$

where ρ_g = gas density at in-situ pressure and temperature, lbm/ft^3;

$K = (9.4 + 0.02M_g)T^{1.5}/(209 + 19M_g + T)$

$X = 3.5 + (986/T) + 0.01M_g$

$Y = 2.4 - 0.2X$

T = in-situ temperature, ^{o}R; and M_g = apparent molecular weight of the gas mixture.

Gas compressibility (c_g). Isothermal gas compressibility can be defined as the change in volume per unit volume of gas for a unit change in pressure, expressed mathematically as follows.

$$c_g = -\frac{1}{V}\left(\frac{\partial V}{\partial p}\right)_T \tag{A33}$$

Using the real gas law to replace volume in the above equations and after proper differentiation, Eq. (A33) becomes as follows.

$$c_g = \frac{1}{p} - \frac{1}{Z}\left(\frac{dZ}{dp}\right)_T \tag{A34}$$

In-situ gas volumetric flow rate. The in-situ gas flow rate can be calculated using the following equation.

$$q_g = [q'_g - q'_o R_s]B_g \tag{A35}$$

Compositional model

The component liquid mole fraction is derived from a single component mole balance and total mole balance and given as,

$$x_i = \frac{z_i}{1 + (V/F)(K_i - 1)} \tag{A36}$$

At thermodynamic vapor-liquid equilibrium, the fugacities of the vapor and liquid for each component are equal. Whitson and Brule (2000) show that this leads to a definition of K-values as the ratio of fugacity coefficients given by Eq. (A37),

$$K_i = \frac{\phi_i^L}{\phi_i^v} \tag{A37}$$

The fugacity coefficients are dependent on the cubic EOS being used. For the cubic Peng Robinson (1976) EOS for the vapor and liquid phases, the fugacity coefficients are given by Eqs. A38 and A39 as,

$$\phi_i^v = \exp\left(\frac{B_{vi}}{B_v}(Z_v - 1) - Ln(Z_v - B_v) + \frac{1}{2\sqrt{2}B_v}\left(\frac{A_v B_{vi}}{B_v} - 2\sum_{j=1}^{n} y_j A_{vij}\right)Ln\left[\frac{Z_v + (1+\sqrt{2})B_v}{Z_v + (1-\sqrt{2})B_v}\right]\right) \tag{A38}$$

$$\phi_i^L = \exp\left(\frac{B_{Li}}{B_L}(Z_L - 1) - Ln(Z_L - B_L) + \frac{1}{2\sqrt{2}B_L}\left(\frac{A_L B_{Li}}{B_L} - 2\sum_{j=1}^{n} x_j A_{Lij}\right)Ln\left[\frac{Z_L + (1+\sqrt{2})B_L}{Z_L + (1-\sqrt{2})B_L}\right]\right) \tag{A39}$$

where $A_{vij} = (1 - k_{ij})\sqrt{A_{vi}A_{vj}}$, $A_{Lij} = (1 - k_{ij})\sqrt{A_{Li}A_{Lj}}$ and all other variables in Eqs. A38 and A39 are given by Whitson and Brule (2000).

Hydrodynamics modeling

In this study, Ansari et al. (1994) mechanistic model is used for the hydrodynamic modeling. The purpose of the hydrodynamic modeling is to predict flow pattern, liquid holdup, and pressure gradient along the wellbore. The following is a summary of Ansari et al. model. The units system used in Ansari et al. model is SI.

Flow pattern prediction

Bubble/slug transition

$$v_{Sg} = 0.333 v_{SL} + 0.25\left[\frac{5.48 g \sigma_L(\rho_L - \rho_g)}{\rho_L^2}\right]^{0.25} \sin\theta \tag{A40}$$

Bubble/dispersed bubble transition

$$[0.725(v_{SL} + v_{Sg})^{-1.12} + 4.15(v_{SL} + v_{Sg})^{-1.62}\sqrt{v_{Sg}}] = \frac{0.487\mu_L^{0.08}\rho_L^{0.52}}{d^{0.48}\sigma_L^{0.1}\sqrt{(\rho_L - \rho_g)g}} \tag{A41}$$

Slug/dispersed bubble transition

$$v_{Sg} = 3.17 v_{SL} \tag{A42}$$

Slug/annular transition. There are three criteria for this transition. For slug flow pattern to occur, at least one of the following three criteria has

to be satisfied. If none of them is satisfied, the flow is annular.

Liquid droplet falling back criterion

$$v_{Sg} = 3.1\left[\frac{\sigma_L g \sin\theta(\rho_L - \rho_g)}{\rho_g^2}\right]^{0.25} \tag{A43}$$

Film bridging criterion

$$[H_{Lf} + \lambda_{Lc}(1 - H_{Lf})] \geq 0.12 \tag{A44}$$

where H_{Lf} is solved implicitly from the following Eq.

$$X^2\frac{(1-f_E)^2}{H_{Lf}}\left(\frac{f_f}{f_{SL}}\right) - \frac{I}{H_{Lf}(1-H_{Lf})^{2.5}} + Y = 0 \tag{A45}$$

where,

$$f_E = 1 - \exp\left[-0.125\left[\left(10^4\frac{v_{Sg}\mu_g}{\sigma_L}\right)\left(\frac{\rho_g}{\rho_L}\right)^{0.5} - 1.5\right]\right] \tag{A46}$$

For $f_E > 0.9$

$$I = (1 + 300\tilde{\delta}_L) \tag{A47}$$

For $fE < 0.9$

$$I = \left[1 + 24\left(\frac{\rho_L}{\rho_g}\right)^{1/3}\tilde{\delta}_L\right] \tag{A48}$$

$$H_{Lf} = 1 - (1 - 2\tilde{\delta}_L)^2 \tag{A49}$$

$$X^2 = \frac{-(dp/dL)_{SL}}{-(dp/dL)_{Sc}} \tag{A50}$$

$$\left(\frac{dp}{dL}\right)_{SL} = -\frac{C_L(\rho_L v_{SL} d/\mu_L)^{-n}(\rho_L v_{SL}^2)}{2d} \tag{A51}$$

$$\left(\frac{dp}{dL}\right)_{Sc} = -\frac{C_c(\rho_c v_{Sc} d/\mu_c)^{-n}(\rho_c v_{Sc}^2)}{2d} \tag{A52}$$

$$v_{Sc} = v_{Sg} + v_{SL}f_E \tag{A53}$$

$$\lambda_{Lc} = \frac{v_{SL}f_E}{v_{Sg} + v_{SL}f_E} \tag{A54}$$

$$\rho_c = \rho_g(1 - \lambda_{Lc}) + \rho_L\lambda_{Lc} \tag{A55}$$

$$\mu_c = \mu_g(1 - \lambda_{Lc}) + \mu_L\lambda_{Lc} \tag{A56}$$

$$Y = \frac{(\rho_L - \rho_c)g\sin\theta}{-(dp/dL)_{Sc}} \tag{A57}$$

Film instability criterion

Eq. (A58) is solved implicitly for H_{Lfmin}, which is then compared with H_{Lf} determined from previous criterion as in Eq (45). If H_{Lf} is greater than H_{Lfmin}, then the film is instable and slug flow occurs.

$$Y - \frac{(2 - 1.5H_{Lf_{\min}})(1-f_E)^2}{H_{Lf_{\min}}^3(1 - 1.5H_{Lf_{\min}})}\left(\frac{f_f}{f_{SL}}\right)X^2 = 0 \tag{A58}$$

Average liquid holdup

The following are the equations of average liquid holdup for each flow pattern:

Bubble flow

$$\left[\frac{5.48g\sigma_L(\rho_L - \rho_g)}{\rho_L^2}\right]^{0.25} H_L^{0.5}\sin\theta - \frac{v_{Sg}}{1 - H_L} + 1.2v_m = 0 \tag{A59}$$

Dispersed bubble flow

$$\lambda_L = \frac{v_{SL}}{v_{SL} + v_{Sg}} \tag{A60}$$

Slug flow

$$H_L = H_{LSU} = \frac{H_{LLS}L_S + H_{LTB}L_{TB}}{L_{SU}} \tag{A61}$$

Annular flow

$$H_L = H_{Lf} + (1 - H_{Lf})\lambda_{Lc} \tag{A62}$$

Pressure gradient

The following are the pressure gradient equations each predicted flow pattern:

Bubble flow

$$\left(\frac{dp}{dL}\right)_T = -\rho_s g \sin\theta - \frac{f\rho_s v_m^2}{2d} \tag{A63}$$

Dispersed bubble flow

$$\left(\frac{dp}{dL}\right)_T = -\rho_n g \sin\theta - \frac{f_n\rho_n v_m^2}{2d} \tag{A64}$$

Slug flow

$$\left(\frac{dp}{dL}\right)_T = \left(\frac{dp}{dL}\right)_{SU} = \left[\left(\frac{L_S}{L_{SU}}\right)\left(-\frac{f_{LS}\rho_{LS}v_m^2}{2d} - \rho_{LS} g \sin\theta\right) + \left(\frac{L_{TB}}{L_{SU}}\right)(-\rho_g g \sin\theta)\right] \tag{A65}$$

Annular flow

$$\left(\frac{dp}{dL}\right)_T = \left(\frac{dp}{dL}\right)_c = \left(\frac{I}{(1 - 2\tilde{\delta}_L)^5}\right)\left(-\frac{dp}{dL}\right)_{Sc} - \rho_c g \sin\theta \tag{A66}$$

Thermodynamics modeling

To model the asphaltene precipitation thermodynamically, two models have been used in this study, namely de Boer et al. (1995) and Wang et al. (2006), which are described as follows.

de Boer et al. (1995) Model

The de-Boer et al. model is based on Hildebrand's asphaltene solubility parameter of the oil and asphaltene (Flory and Huggins). The solubility (S) is expressed as follows,

$$S = \exp\left\{-1 + v_a\left[\frac{1}{v_o} - \frac{(\delta_a - \delta_o)^2}{RT}\right]\right\} \times C \tag{A67}$$

where S = asphaltene solubility, m^3/m^3, v_a = asphaltene molar volume, m^3/kmol, v_o = oil molar volume, m^3/kmol, δ_a = asphaltene solubility parameter, $Pa^{1/2}$, δ_o = oil solubility parameter, $Pa^{1/2}$, C = Correction parameter for asphaltene polimerization and asphaltene-resin interaction, R = gas constant = 8314, m^3Pa/kmole-K, T = temperature, K.

For simplicity, de-Boer et al. correlated the solubility with in-situ crude oil density, resulting in the well-known de-Boer plot in which the y-axis of the difference between reservoir pressure and bubble-point pressure (p_{res}-p_b), and x-axis of the in-situ crude oil density. de-Boer et al. plot is developed for a single point asphaltene precipitation prediction in reservoirs. However, in this study de-Boer et al. model was extended for the application of asphaltene precipitation along wellbore, where the in-situ crude oil density is along the wellbore and plotted using the boundaries of de-Boer plot. The new de-Boer plot in wells developed in this study is shown in Fig. 3. In this figure, the two vertical lines are the boundaries of asphaltene risk region corresponding to as specific (p_{res}-p_b).

Wang et al. (2006) Model

The model consists of two sub-models, namely asphaltene solubility parameter at instability condition (δinstability), and live-oil solubility parameters (δlive-oil), given in Eqs. A68 and A72, respectively.

$$\delta_{instability} = \delta_{onset,n-C7} - 0.0128(T_r - T_m) - 0.146(v_{n-C7}^{1/2} - v_{light}^{1/2}) \tag{A68}$$

where $\delta_{instability}$ = asphaltene solubility parameter at instability condition ($MPa^{1/2}$), $\delta_{onset,n\text{-}C7}$ = onset solubility parameter measured at temperature from n-C7 titration experiment ($MPa^{1/2}$), T_r = reservoir temperature (°C), T_m = solubility measured temperature (°C). v_{n-C7} = n-heptane molar volume (cm^3/mol), and v_{light} = light ends molar volume (cm^3/mol), which are given, respectively, in Eqs. A69 and A70,

$$v_{nC7}^{1/2} = 4.01 \times 10^{-5}T_r + 4.6 \times 10^{-3}T_r + 11.97 \tag{A69}$$

$$v_{light} = \frac{1.33 \times 10^5(B_o - B_{o(T_r,p_{sc})})}{R_s} \tag{A70}$$

where B_o = formation volume factor (bbl/STB), R_s = solution GOR (scf/STB), and $B_{o(Tr,psc)}$ = formation volume factor at reservoir temperature and standard pressure (bbl/STB). The B_o and R_s in this study are calculated using Kartoatmodjo and Schmidt (1991) black-oil model and at pressures along wellbore predicted by Ansari et al. two-phase mechanistic model. In this study, using the data reported by Wang et al. (2006), the onset solubility parameter in Eq. (A69) is correlated with API gravity as,

$$\delta_{onset,n-C7} = 0.0255\gamma_{API} + 15.51 \tag{A71}$$

where γ_{API} = API gravity. Eq. (A71) can be used to estimate the onset solubility parameter in the case of no n-C7 titration experimental measurement available, as in the field cases validated in this study. The second sub-model of Wang et al. is the live oil-solubility parameter model given as,

$$\delta_{live-oil} = \frac{1}{B_o}\delta_{STO} + 2.904\left(1 - \frac{1}{B_o}\right) + 3.91 \times 10^{-4}\left(\frac{R_s}{B_o}\right)R_{light} \tag{A72}$$

where δ_{STO} = solubility parameter for stock-tank oil at standard conditions ($MPa^{1/2}$), and R_{light} = molar refraction of light ends (cm^3/mol) given as,

$$\delta_{STO} = -(0.078)\gamma_{API} + 20.426 \tag{A73}$$

$$R_{light} = (15.9)\left(\frac{x_{C_1-C_3}}{x_{C_1-C_6}}\right) + 23.0 \tag{A74}$$

The $(x_{C1}\text{-}x_{C3})/(x_{C1}\text{-}x_{C6})$ = the ratio of mole fraction of C_1-C_3 to mole fraction of C_1-C_6 (−).

References

Abdallah, D., Al-Basry, A., Zwolle, S., et al., 2010. Asphaltene studies in on-shore Abu Dhabi oil fields. In: PART II: Investigation and Mitigation of Asphaltene Deposition – a Case Study. Paper Presented in Abu Dhabi International Petroleum Exhibition and Conference, Abu Dhabi. 1–4 November. SPE-138039-MS.

Abuie, A., Shirdel, M., Darabi, H., et al., 2015. Modeling asphaltene deposition in the wellbore during gas lift process. In: SPE 174067, Paper Presented at SPE Western Regional Conference, Garden Grove, pp. 27–30 April. SPE-174067-MS.

Alapati, R., Joshi, N., 2013. New test method for field evaluation of asphaltene deposition. In: Paper Presented in Offshore Technology Conference, Houston, pp. 6–9 May 20. OTC-24168.

Alkafeef, S., Al-Medhadi, F., Al-Shammari, A., 2005. A simplified method to predict and prevent asphaltene deposition in oilwell tubing: field case. *SPE Prod Fac* (May) SPE-84609-PA.

Ansari, A.M., Sylvester, N.D., Sarica, C., et al., 1994. A comprehensive mechanistic model for upward two-phase flow in wellbores. SPE Prod. Eng. 9 (2), 143–152 SPE-20630-PA.

de Boer, R., Leerlooyer, K., Eigner, M., van Bergen, A., 1995. Screening of crude oils for asphalt precipitation: theory, practice, and the selection of inhibitors. SPE Prod. Fac. 2, 55–61.

Burke, N., Hobbs, R., Kashou, S., 1990. Measurement and modeling of asphaltene precipitation. SPE J SPE-18273-PA.

Firoozabadi, A., 1999. Thermodynamics of Hydrocarbon Reservoirs. McGraw-Hill, New York.

Hashmi, S., Firoozabadi, A., 2016. Effective removal of asphaltene deposition in metal-capillary tubes. SPE J. Oct SPE-166404-PA.

Hirschberg, A., De Jong, L., Schipper, B., Meijers, J., 1984. Influence of temperature and pressure on asphaltene flocculation. SPE J SPE-11202-PA.

Kabir, C.S., Jamaluddin, A.K., 2002. Asphaltene characterization and mitigation in south Kuwait's marrat reservoir. SPE Prod Fac (November) SPE-53155-PA.

Kartoatmodjo, R.S.T., Schmidt, Z., 1991. New correlations for crude oil physical properties. SPE eLibrary Pap SPE-23556-MS.

Kurup, A., Buckley, J., Wang, J. et al.. 2012. Asphaltene deposition tool: field case application protocol. Paper Presented in Offshore Technology Conference, Houston, April 30, 2012. OTC-23347.

Leontaritis, K.J., 1989. Asphaltene deposition: a comprehensive description of problem manifestations and modeling approach. In: Paper Presented at the Production Operation Symposium, Oklahoma City, March. SPE-18892-MS.

MacMillan, D., Tackett, J., Jessee, M., et al., 1995. A unified approach to asphaltene precipitation: laboratory measurement and modeling. J. Pet. Technol SPE-28990-PA.

Mansoori, G., 1997. Modeling of asphaltene and other heavy organic depositions. J Pet Sci Eng.

Speight, C., 1991. Chemistry and Technology of Petroleum. Marcel & Dekker Inc.

Sulaimon, A., Govindasamy, K., 2015. New correlation for predicting asphaltene deposition. In: Paper Presented in SPE/IATMI Asia Pacific Oil and Gas Conference and Exhibition, Bali, Indonesia, pp. 20–22 October. SPE-176436-MS.

Takhar, S., Ravenscroft, P., Nicoll, D., 1995. Prediction of asphaltene deposition during production – model description and experimental details. In: Paper Presented at SPE European Formation Damage Conference, SPE-30108-MS.

Wang, J., Creek, J., Buckley, J., 2006. Screening for Potential Asphaltene Problems. Paper presented at SPE ATCE, San Antonio SPE-103137-MS.

Whitson, C.H., Brule, M.R., 2000. Phase Behavior Vol. 20 Monograph Series, Society of Petroleum Engineers, Richardson, Texas.

Yen, T., 1995. The colloidal nature of asphaltics. Paper presented at the 1st. In: Symposium on Colloid Chemistry in Oil Production: Asphaltenes and Wax Deposition, Rio de Janeiro, November.

Glossary

B = : Formation volume factor, bbl/stb
c = : compressiblity, $m.s^2$/kg
C = : Correction parameter, Constant
f = : Moody friction factor (−)
f_E = : liquid entrainment fraction (−)
g = : acceleration of gravity, m/s^2
GOR = : Gas oil ratio, scf/STB
H_L = : liquid holdup (−)
k = : Binary Interaction Parameter (BIP)
K = : Equilibrium constant (−)
L = : Length
M_w = : molecular weight, M/mol, kg/kmol
q = : volumetric flow rate, m^3/d, ft^3/d
p = : Pressure, Mpa, psi
R = : gas constant, J/kg-kmol; Molar refraction, cm^3/mol
R_s = : Solution gas oil ratio, scf/STB
S = : Asphaltene solubility, m^3/m^3
T = : temperature, °C, °F
v = : velocity, m/s; Molar volume, cm^3/mol
x = : Mole fraction, mol/mol
X = : Lockhard-Martinelli parameter (−)
Y = : Inclination angle number (−)
Z = : Z-factor

Greek Letters

δ = : Solubility parameter, $MPa^{1/2}$
$\tilde{\delta}$: = dimensionless film thickness (−)
γ = : Specific gravity
λ = : no-slip holdup (−)
μ = : absolute viscosity, kg/m-s, cp
θ = : inclination angle, degrees or radian
ρ = : Density, kg/m^3, lbm/ft^3
σ = : surface tension, kg/s^2, dyne/cm

Subscripts

a = : Asphaltene
API = : API gravity
b = : bubble point
c = : core
C = : calculated
d = : diameter
f = : film, frictional
g = : gas
G = : guessed
$light$ = : Light ends
L = : liquid
LS = : liquid slug
m = : Measured, mixture
n = : no-slip
o = : Oil
p = : n-alkane precipitant
res = : Reservoir
Re = : Reynolds
Sg = : superficial gas
SL = : superficial liquid
STO = : Stock tank oil
SU = : slug unit
T = : Total
TB = : Taylor bubble
v = : vapor
wh = : wellhead